Nano Energy (2015) 12, 698–708

Available online at www.sciencedirect.com

ScienceDirect

journal homepage: www.elsevier.com/locate/nanoenergy

RAPID COMMUNICATION

Self-stacked nitrogen-doped carbon nanotubes as long-life air electrode for sodium-air batteries: Elucidating the evolution of discharge product morphology

Qian Sun, Hossein Yadegari, Mohammad N. Banis, Jian Liu, Biwei Xiao, Biqiong Wang, Stephen Lawes, Xia Li, Ruying Li, Xueliang Sun*

Department of Mechanical and Materials Engineering, University of Western Ontario, London, ON, Canada N6A 5B9

Received 18 December 2014; accepted 8 January 2015
Available online 21 January 2015

KEYWORDS
Na-Air Battery;
NCNT;
Cycling performance;
Discharge product morphology;
Catalyst activity

Abstract
Self-stacked nitrogen-doped carbon nanotubes (NCNTs) and pristine carbon nanotubes (CNTs) on commercial porous polypropylene substrates have been applied as air electrodes for sodium-air batteries (SAB). Both NCNT and CNT air electrodes exhibit highly reversible electrochemical activities and large capacities under low current densities in SABs, while NCNT electrodes show much higher rate performance and extended cycling life under high current densities. The superior electrochemical behavior of NCNT electrodes is attributed to the robust network of aligned NCNTs, which enables rapid oxygen and liquid electrolyte transport while accommodating the volume change originating from discharge product aggregation during cycling. Moreover, uniform coverage of the discharge product has been observed on the NCNT air electrodes, in contrast to the random and discrete dispersion of discharge product on the CNT air electrodes. The unique morphologies and growth mechanism of discharge products on NCNT electrodes are believed to be due to the outstanding catalytic activity of the nitrogen-doped sites in the NCNTs, which play a critical role in the high cycling stability of NCNT air electrodes for SABs.

*Corresponding author. Tel.: +1 519 661 2111 x 87759; fax: +1 519 661 3020.
E-mail address: xsun@eng.uwo.ca (X. Sun).

http://dx.doi.org/10.1016/j.nanoen.2015.01.018
2211-2855/

Introduction

The development of sustainable and renewable energy storage devices has been greatly advanced in recent decades, due to the concerns of increasing greenhouse gas emissions (e.g. CO_2) as a consequence of fossil fuel consumption. Electric vehicles (EVs) and hybrid electric vehicles (HEVs) have therefore received tremendous attention as a potential solution to diminish the impact of humankind on the environment. Up to now, Lithium-ion Batteries (LIBs) are one of the main choices for EV and HEV applications. However, EVs based on LIBs in the state-of-art are still restricted by insufficient specific energy densities for long-distance or large power output applications [1]. Recently, alkali metal-air batteries, i.e. Lithium-Air Batteries (LABs) [2-6], Sodium-Air Batteries (SABs) [7-9], and Potassium-Air Batteries (PABs) [10], have attracted increasing interest as potential alternatives for high performance power sources in future. Compared with other chemical power supplies, these alkali metal-air cells present high voltage outputs as a result of the combination of high oxygen reduction potential and low A^+/A potentials(A=Li, Na, and K), which also exhibit large specific capacities due to the light atomic weights of Li, Na, K, and O elements. Thus, alkali metal-air batteries conceive great potential for the applications as high energy output power sources in the future.

In contrast to the massive number of studies on LABs over the past few decades, the nature of SABs has remained unrevealed until recently. SABs are constructed from the combination of high energy density air breathing cathodes with inexpensive and abundant metal sodium anodes, making them promising candidates for future power sources due to their low costs, large gravimetric capacities and high power outputs. In addition, the abundance of elemental sodium in the Earth ensures the widespread adoption of this novel energy conversion system feasible.Nevertheless, despite the similar characteristics of element Li and Na, the significant distinction between the thermodynamic stabilities of their peroxides(Li_2O_2 and Na_2O_2) and superoxides (LiO_2 and NaO_2) contributes to their downright different electrochemical behaviors. Much lower overpotentials between the charge and discharge voltages of SABs compared with LABs have been observed in previous studies [8,9,11-17], which are greatly favored for practical applications. A recent theoretical calculation study points out that the lower overpotentials in SABs are assigned to the differences between the chemical properties of both sodium superoxides and peroxides, and lithium peroxides [18]. Thus, SABs have been attracting increasing research interest from both theoretical and practical standpoints. However, most SABs reported so far are limited by their insufficient cycling stabilities (generally within 10 cycles), except for very few reports tested under pure oxygen [9,16,17]. Therefore, it is critical to explore novel, long-term sustainable air electrodes, with the aim of boosting the development of SABs.

Considering the inherent similarity between the principles of LABs and SABs [19], it is natural to pursue the possible solutions to overcome the obstacles of SABs from the experience of LABs. It has been numerously reported that the design of air electrodes [20-22] and the morphologies of the discharge products [23-25] play critical roles in the cycling performance of LABs. Pristine carbon nanotubes (CNTs) [26] and nitrogen-doped carbon nanotubes (NCNTs) [27,28] have already been intensively studied as potential air electrode materials for LABs, and exhibited an extended cyclic life. Recently, Zhang et al. [11] reported a free-standing CNT paper air electrode for SABs, delivering large first discharge capacity, but was still limited to a cyclic life below 10 cycles. On the other hand, it has been widely reported that NCNT air electrodes exhibit improved performance compared with CNT counterparts in LABs [27,28]. Nevertheless, to our best knowledge, NCNT air electrodes have not been reported to be tested as an air electrode material for SAB so far. In addition, few of the previous studies on SABs have focused on the relationship between the discharge product morphologies and the performance of the air electrodes.

Herein we developed a new design of air electrodes for SABs based on a novel fabrication approach of self-stacking NCNTs or CNTs on commercial porous polypropylene (PP) separator substrates. Both NCNT and CNT air electrodes presented reversible electrochemical activities and relevant large capacities under low current density, while NCNT electrodes showed much better performance and extended cyclic lives up to 50 cycles under high current densities. This superior electrochemical behavior of NCNT electrodes is attributed to the robust network woven by the aligned NCNT units, enabling rapid oxygen and liquid electrolyte transportation. In addition, the morphological differences between the discharge products of NCNT and CNT air electrodes have been observed. The unique morphologies of uniform discharge products of NCNT air electrodes are related to the catalytic activity of the nitrogen-doped sites in the NCNTs, and is a critical determining factor of their extended cyclic lives of the SABs.

Experimental

Preparation of nitrogen-doped carbon nanotubes

Aligned NCNTs were fabricated following the method previously reported by our group [29]: NCNTs were fabricated by a floating catalyst chemical vapor deposition (FCCVD) method. Imidazole was chosen as the carbon and nitrogen source and ferrocene was used as the catalyst precursor. Ferrocene decomposes into iron at 850 °C, which acts as the catalyst for carbon nanotube growth and introduces nitrogen atoms into the graphite layers of the carbon nanotubes to form NCNTs.

Preparation of NCNT and CNT air electrodes

The preparation process for NCNT and CNT air electrodes are schematically shown in Figure 1. NCNT and CNT air electrodes were fabricated by a two-step process: at first, the NCNT or CNT powders were mixed with PVDF binder and then uniformly dispersed in organic solvent by sonication; then the mixtures were dipped and spread on a commercial PP porous separator film substrate. Upon evaporation of the organic solvent, the NCNTs or CNTs stacked together and formed a hierarchical nanostructured air electrode

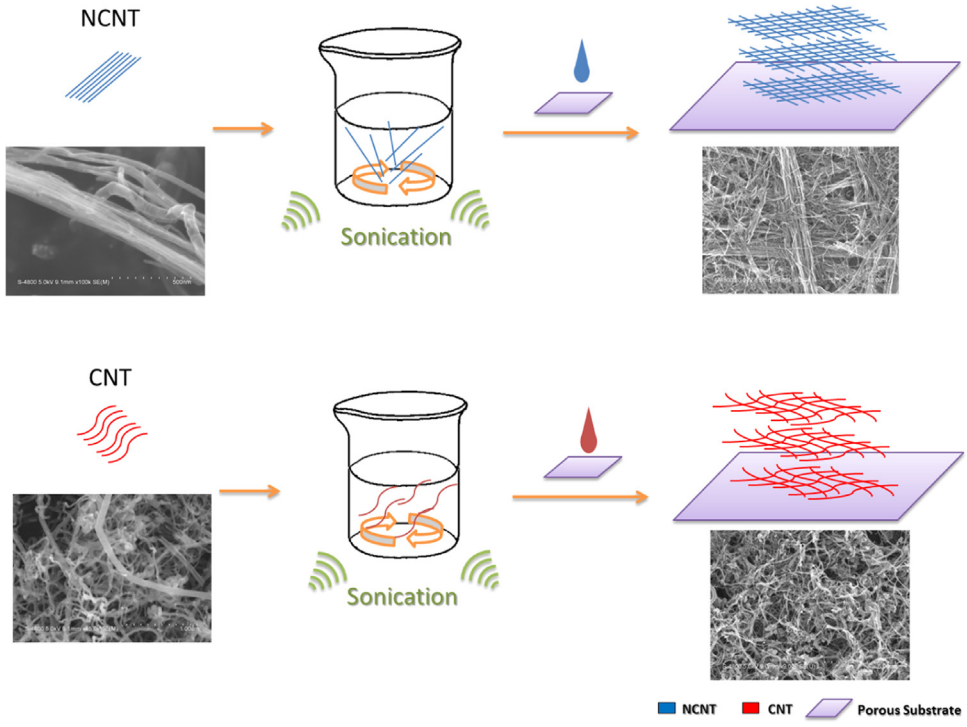

Figure 1 Schematic diagram of fabrication of NCNT and CNT air electrodes by the combination of sonication dispersion and self-stacking processes. SEM images of original NCNT, pristine CNT, and both corresponding air electrodes are also included.

material. Commercial CNT powders are directly used without further treatment. In a typical process, 80 mg NCNT or CNT powder were mixed with 20 mg polyvinylidene fluoride (PVDF) binder and then uniformly dispersed in 10 mL N-methy-2-pyrrolidone (NMP) by 8 h of stirring and 12 h of sonication. Then the NCNT–PVDF or CNT–PVDF mixtures were dipped and spread on Celgrid 3501 thin film substrate to form the self-stacking NCNT and CNT air electrodes, respectively.

Physical characterizations

Hitachi S-4800 field-emission scanning electron microscope (SEM) operated at 10.0 kV was used for the observation of the morphologies of the pristine materials and air electrodes. X-Ray Diffraction (XRD) patterns were recorded using a Bruker D8 Advance (Cu-Kα source, 40 kV, 40 mA) spectrometer. N_2 adsorption/desorption isotherms were achieved with a surface area and pore size analyzer (Folio Micromeritics TriStar II).

Electrochemical measurements

The sodium-air batteries were tested with Swagelok-type cells composed of a metallic sodium foil anode, PP separator (Celgard 3501), and NCNT or CNT air electrode, with a stainless steel mesh current collector on the top. The electrolyte was comprised of 0.5 M sodium triflate ($NaSO_3CF_3$, Aldrich) dissolved in diethylene glycol diethyl ether (DEGDME, Aldrich). The DEGDME solvents were dried with molecular sieves (4 Å, Aldrich) for at least one month before use. The discharge/charge characteristics were performed using an Arbin BT-2000 battery station in a sealed box filled with a 1.0 atm dried air atmosphere at room temperature (25 °C). Electrochemical impedance spectroscopy (EIS) measurements were carried out with a multi potentiostats (VMP3, Biologic).

Results and discussion

The SEM images of NCNTs, pristine CNTs, NCNT and CNT air electrodes are shown in Figure 1. It is important to note that the NCNT air electrode displays a highly organized layer-by-layer arrangement, compared to the fully disordered structure of the CNT electrode. From the cross-sectional SEM images (see Figure S1), this distinction between the two air electrode materials is further evidently revealed. This should probably be attributed to the aligned characteristic of the NCNT units, which were grown to tens of micrometers and are hard to bend (Figure S2). Thus, after dispersion by ultrasonication, the NCNT units tend to stack together layer by layer instead of coiling around each other. In contrast, due to the curved nature of pristine CNTs, the morphology of the CNT air electrode appeared to be twisted and hairy. This unique structure of the NCNT air electrode not only provides interval spacing among the NCNTs, which are beneficial for oxygen transport and immersion of liquid electrolyte, but also constructs a robust network to accommodate discharge products, which can be durable for long-term cycling of the cell. The concentration of N species in NCNTs is determined to be around 10% by EDS analysis. In addition, it can be observed from the SEM that NCNT air electrode has a densely packed structure, while pristine CNT air electrode has a loose structure. The pore structure

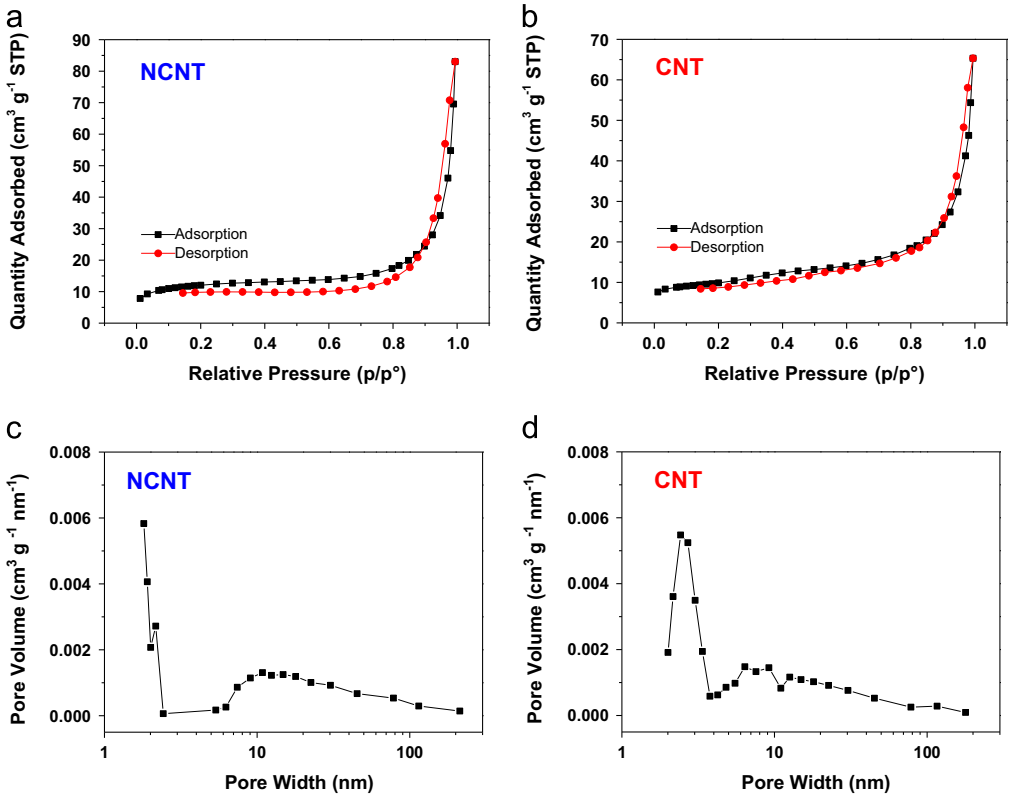

Figure 2 Nitrogen adsorption/desorption isotherms of (a) NCNT and (b) CNT materials; pore size distribution plots for (c) NCNT and (d) CNT materials.

plays an important role in the performance of air electrodes on their catalytic activities and also provides space for the accommodation of the discharge products. In order to further reveal information on their pore distributions, N_2 adsorption/desorption experiments have been carried out on both NCNT and CNT materials (Figure 2(a and b)). The Brunauer-Emmett-Teller (BET) surface areas of NCNTs and CNTs are measured to be 42.1151 and 33.8975 $m^2\,g^{-1}$, respectively. Despite their close BET areas, the pore distributions of NCNTs and CNTs are found to be different. NCNTs mainly contain micropores with diameters below 2 nm and also mesopores over a wide range of 5-100 nm. In contrast, CNTs have a much narrower mesoporous structure composing of pores with diameters around 2-3 and 8-9 nm as well as some macropores. These differences between the pore structures of NCNTs and CNTs can also result in and will be also discussed in the following part.

The flexible and free-standing NCNT air electrodes were cut into small discs for testing in SABs under a dried air environment (Figure S3). The typical voltage profiles for NCNT air electrodes are shown in Figure 3, while the electrochemical behavior of SABs with CNT air electrode are shown in Figure S4 for comparison. Figure 3(a) shows the first discharge and charge curves of NCNT air electrodes in SABs at different current densities. The NCNT air electrode delivers a discharge capacity of 1887, 1476, 988 and 572 mAh g^{-1}, at 25, 50, 130 and 600 mA g^{-1}, respectively. These values of the gravimetric discharge capacities are comparable with their performance in LABs [27-29]. During the first discharge process, the NCNT air electrode presents a single voltage plateau around 2.13, 2.06, 2.04, and 1.98 V, at 25, 50, 130 and 600 mA g^{-1}, respectively. The polarization voltage between charging and discharging profiles is found to be as low as 0.2 V at a current density of 25 mA g^{-1} and gradually rises to 0.3 V as the current density increases to 130 mA g^{-1}. No obvious plateau can be found in the charging curve of the cell cycling at 600 mA g^{-1}, due to the increasing polarization under high current densities.

The typical discharge and charge curves of a SAB with NCNT air electrode at a current density of 130 mA g^{-1} are shown in Figure 3(b). It can be observed that all the subsequent discharging curves also exhibit voltage plateaus around 2.0 V with similar shapes as the first discharging curve. With increasing cycle number, the overpotential of the charging curves significantly increased. It should be noted that in every cycle the corresponding charge capacity of the cell is slightly less than the discharge capacity (inset of Figure 3(b)). This indicates that trace amounts of the discharge products cannot be fully decomposed during each electrochemical charging process. These residual discharge products may gradually aggregate and eventually lead to the failure of the SABs, as previously reported for SABs in pure oxygen environment [9,14]. A similar phenomenon is also observed in the CNT air electrodes (Figure S4(a) and (b)). The charge/discharge curves of CNT air electrodes reported herein are similar to those of SABs with CNT powder electrodes previously reported [11]. They also reported that self-standing CNT air electrodes suffered from a short cycling live of 3 cycles under full charge and discharge cycling with a high first discharge capacity of about 7500 mAh/g, while better results were achieved by cycling the cell under restricted depth of discharge for

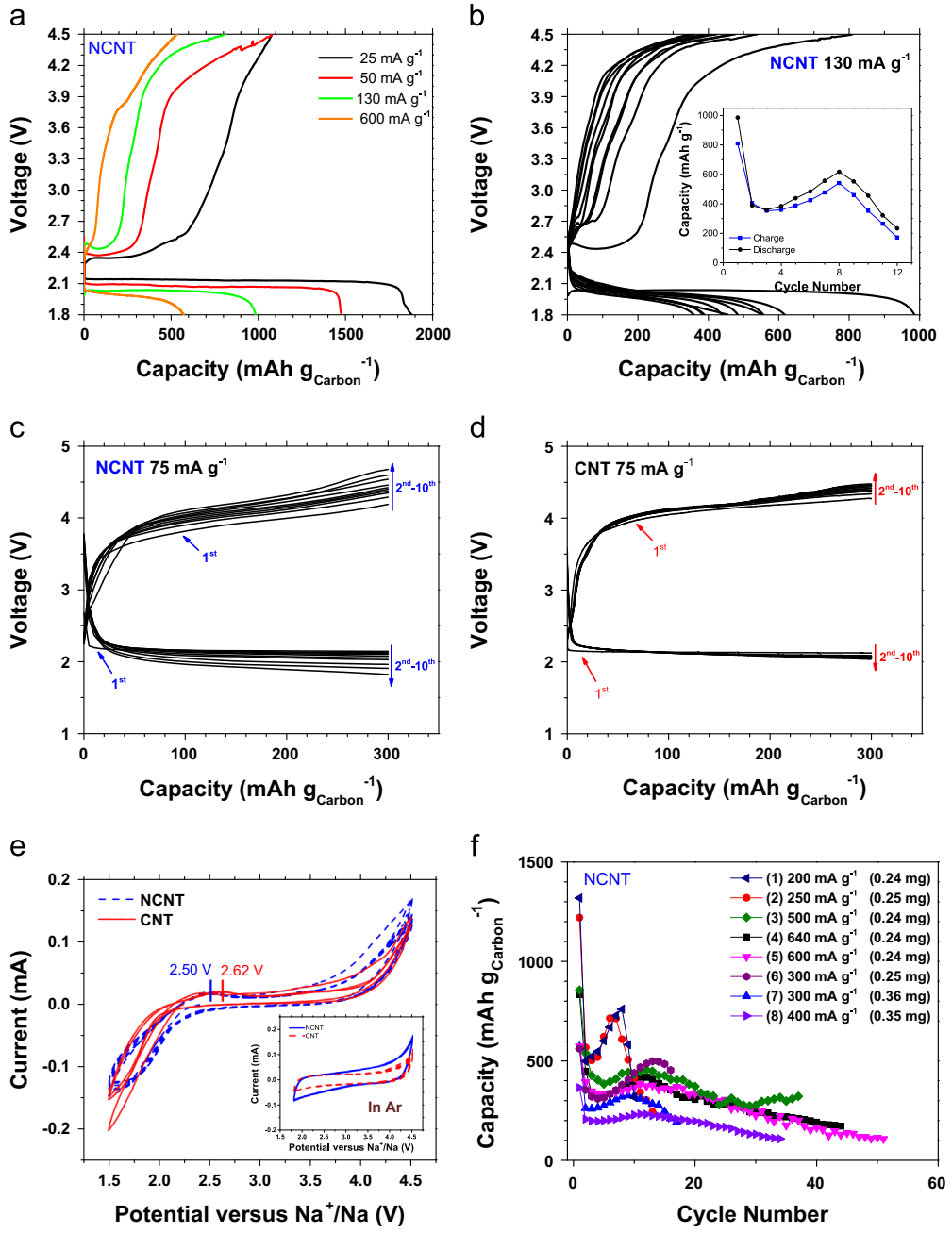

Figure 3 (a) First cycle charge and discharge curves of sodium-air batteries with NCNT electrode at current densities of 25, 50, 130, and 600 mA g^{-1}; (b) cycling profiles of a typical sodium-air battery with NCNT electrode at a current density of 130 mA g^{-1}; inset: the cycling retention of the cell versus cycle number; limited discharge and charge curves of sodium-air batteries using (c) NCNT and (d) CNT material recorded at a constant current density of 75 mA g^{-1}; (e) the first three CV curves of the SABs with NCNT and CNT air electrodes in the presence of dried air between 1.5 and 4.5 V; inset: the CV curves of the cells with NCNT and CNT air electrodes in the presence of argon ambient at a scanning rate of 0.1 mV s^{-1}; (f) evolution of cycling retention of the sodium air batteries at different current densities of 200 mA g^{-1} (0.24 mg), 250 mA g^{-1} (0.25 mg), 500 mA g^{-1} (0.24 mg), 600 mA g^{-1} (0.24 mg), 640 mA g^{-1} (0.24 mg), 300 mA g^{-1} (0.25 mg), 300 mA g^{-1} (0.36 mg), and 400 mA g^{-1} (0.35 mg). The weights of active materials are noted.

7 cycles. Although the discharging capacity of the self-stacked CNT air electrode reported herein is lower, the cell maintained 13 cycles under full discharging and charging. These facts imply that the morphology of air electrodes, even those based on the same materials, may result in different electrochemical performance.

The NCNT and CNT air electrodes were also investigated by cycling at low depth of discharge (DOD), with a capacity cut-off of 300 mAh g^{-1}. Figure 3(c) and (d) illustrates the discharge/charge profiles of NCNT and CNT air electrodes, respectively, during the initial 10 cycles at a current density of 75 mA g^{-1}. For the NCNT air electrode, the discharge and

charge plateaus fall into the voltage range of 2.22–1.82 V and 4.17–4.66 V, respectively, while for the CNT air electrode, the discharge and charge voltage plateaus are in the range of 2.15–2.04 V and 4.42–4.49 V, respectively. Therefore, the NCNT air electrode displays higher bifunctional electrocatalytic activity towards both ORR and OER than the CNT counterpart. A similar phenomenon was also previously found in LABs [23–25]. It is believed that the nitrogen doping sites in NCNTs might induce more defects for oxygen adsorption and electron transfer, where ORR preferentially takes place [23].

Cyclic voltammetry (CV) measurements were carried out to further examine the OER and ORR activities of NCNT and CNT air electrodes. The CV curves of NCNT and CNT electrodes in a dried air and an argon atmosphere are shown in Figure 3(e). No obvious current peak related to faradic redox reaction was observed in the CVs of both NCNT and CNT electrodes in the argon atmosphere (inset of Figure 3 (e)). However, the NCNT and CNT electrodes exhibit apparently different CV curves under the dried air environment. The anodic and cathodic peaks of ORR and OER are located at 1.80 V and 2.50 V separately for NCNT air electrode, and 1.68 V and 2.62 V for CNT air electrode, respectively. The shifting of the ORR to higher voltages and OER to lower voltages indicates improved electrocatalytic activity of NCNT air electrodes towards both OER and ORR compared with CNT air electrodes. The difference between the voltage of corresponding anodic and cathodic peaks was around 0.1 V, which is consistent with the charge and discharge results above.

The cycling performance of NCNT air electrodes was evaluated at different current rates and the results are shown in Figure 3(f). All of the cells cycled at the current densities ranging from 200 to 640 mA g^{-1} exhibited good cycling performance for at least 10 cycles. Two cells cycling at 600 mA $g^{-1}$and 640 mA g^{-1} sustained 44 and 50 cycles before their capacities dropped to below 100 mAh g^{-1}, respectively. However, the CNT air electrodes showed neither good cycling stabilities nor reasonable reversible capacities. The cycling performance of the CNT air electrode under 200 mA g^{-1} is shown in Figure S4(c). Thus, it can be clearly concluded that NCNT air electrodes show much better electrochemical performance than their CNT counterpart under high current rates. It should be noted that such a huge distinction between the rate performance of NCNT and CNT electrodes is contributed to by the slight difference between their OER and ORR activities, as shown above; this will be further addressed in the following section. In addition, a common phenomenon can be witnessed: the discharge capacities of the cells increased after the second cycle and achieved a maximum value between 8 and 12 cycles. This might be due to repeated discharge product aggregation during discharging and gas releasing during charging, creating more holes and gas diffusion tunnels inside the NCNT electrodes.

Generally, the possible electrochemical reactions involved in a SAB can be summarized by the following equations. The theoretical potentials for the electrochemical reactions in SABs yielding the NaO_2, Na_2O_2 and Na_2O products are also given based on the calculation of Gibbs free energy data and the thermodynamic equation $\Delta G = -n$FE [8]:

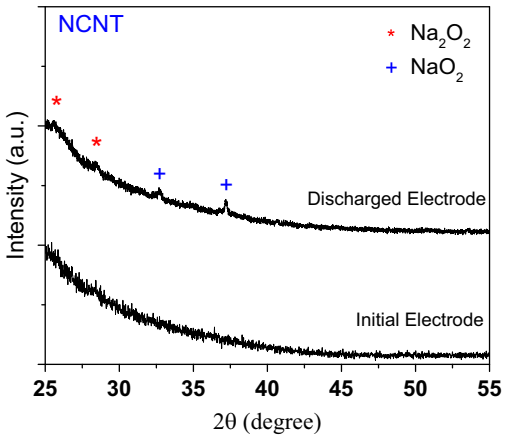

Figure 4 XRD patterns of initial and discharged NCNT air electrodes at a current density of 75 mA g^{-1}.

$$Na^+ + e^- + O_2 \rightarrow NaO_2 \qquad E^0 = 2.26\ V \qquad (1)$$

$$2Na^+ + 2e^- + O_2 \rightarrow Na_2O_2 \qquad E^0 = 2.33\ V \qquad (2)$$

$$4Na^+ + 4e^- + O_2 \rightarrow 2Na_2O \qquad E^0 = 1.95\ V \qquad (3)$$

The electrode potentials corresponding to the formation of NaO_2 and Na_2O_2 have very close values (2.26 V and 2.33 V). Up to now, the discharge products of SABs have been reported to be Na_2O_2 with Na_2CO_3 [8], NaO_2 [9,14,17], $Na_2O_2 \cdot 2H_2O$ [13], or Na_2O_2 [12,15] in different studies, respectively. In this study, the discharge products of NCNT air electrodes were identified with XRD. In Figure 4, clear diffraction peaks are observed at 25.62°, 28.42°, 32.6°, and 37.2°, for a NCNT electrode discharged at a current density of 200 mA g^{-1}. The first two peaks can be attributed to (101) and (110) facets of Na_2O_2 (JCPDS 74-0895), and the latter two can be assigned to (020) and (111) facets of NaO_2 (JCPDS 74-0208). The XRD result reveals that the discharge products of the SAB with NCNT air electrode under dried air condition are the mixture of Na_2O_2 and NaO_2.

It is believed that different experimental conditions can lead to discrepancies in the electrochemical behavior of SABs [17]. In this study, dried air is adopted as the oxygen source (same as Refs. [8] and [12]) instead of pure oxygen as in some other studies (e.g. Refs. [9,11,13–17]). It should be noted that even in the studies on LABs, the directly use of air as oxygen source will lead to poorer electrochemical behaviors and still remains a challenging issue [30,31]. It is recently reported that SABs form negligible side products, except for sodium oxide under pure oxygen ambient, and thus undergo a more "clean" chemistry than LABs to form pure NaO_2 [32]. Meanwhile, it is also reported that alternating pure O_2 gas to 80%Ar+20%O_2 mixed gas as oxygen sources can greatly diminish the formation of NaOH in the discharge product and improve the cycling stabilities of SABs [33]. On the other hand, theoretical calculation studies [34] suggest that discharge products NaO_2 and Na_2O_2 exhibit different stability under specific experimental conditions. NaO_2 particles with large diameters are not stable at 1 atm atmosphere. It is suggested that the stabilizing size of NaO_2 particles is restricted to several nanometers [34]. In the current study, due to the other

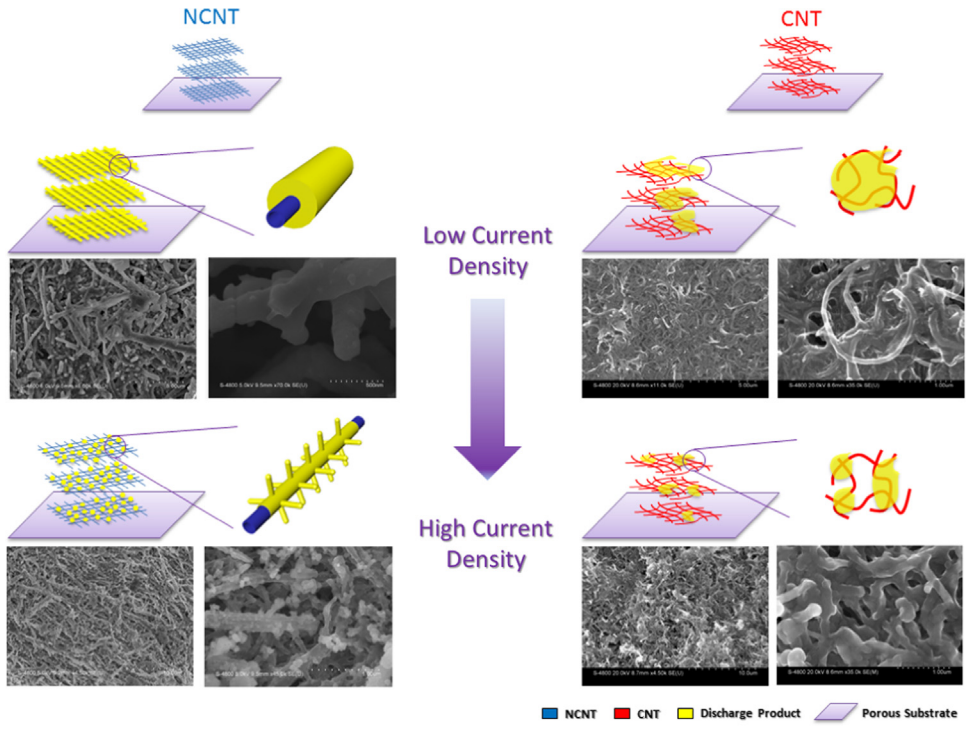

Figure 5 Morphology of discharge products of the sodium-air batteries using NCNT and CNT air electrodes under low (50 mA g^{-1}) and high (300 mA g^{-1}) current densities; schematic diagrams of these discharge products are also included.

existing components other than oxygen in the dried air (e.g. CO_2), sodium oxide discharge products may be contaminated with side products such as Na_2CO_3, which can only be decomposed under higher voltage [8]. Thus, a SAB with CNT air electrode under pure oxygen was also tested in this research for comparison and the results are shown in Figure S4(d). It can be observed that the discharge plateau is located at 2.2 V, while most of the discharge products decomposed at around 2.35 V. This result is consistent with other reports where sodium superoxide (NaO_2) was found to be the main discharge product under pure oxygen gas [9,14]. The transformation of sodium superoxide to sodium peroxide or sodium carbonate can be expressed by the following equations [17]:

$$2NaO_2 = Na_2O_2 + O_2 \quad (4)$$

$$4NaO_2 + 2CO_2 = 2Na_2CO_3 + 3O_2 \quad (5)$$

$$2Na_2O_2 + 2CO_2 = 2Na_2CO_3 + O_2 \quad (6)$$

It should also be noted that reactions (5) and (6) are useful to facilitate a primary SAB which focuses on the capture of greenhouse gas CO_2 from the atmosphere [35]. In this study, the discharge products were found to be a mixture of superoxide and peroxide, which may result from both reaction (2) and reaction (4), implying the chemistry of SABs is rather complicated. Synchrotron based characterizations is going to be carried out by our group to further reveal the reaction mechanism of NCNT based air electrode materials for SABs and will be presented in another work.

Figure 5 shows SEM images and schematic drawings of the morphologies of discharge products and their dispersion on NCNT and pristine CNT electrodes. The morphology of the discharge products on CNT air electrodes is similar to that previously reported by Zhou's group [11]. The morphologies of the discharge products on the CNT air electrodes under both high and low current densities are quite similar, but not as uniform as those on NCNTs. The cross-sectional SEM images of discharged CNT air electrodes (Figure S5) provide more evidence. In contrast, it can be seen that the discharge products were uniformly deposited on the entire NCNT air electrodes, but presented significantly different morphologies under high and low current densities (Figure S6). Under low current densities, the discharge products uniformly covered the whole surface of the NCNTs forming a "core-shell" structure, while under high current densities, the discharge products exist as nanorods on the surface of the NCNTs. This phenomenon is confirmed by the cross-sectional SEM view of the discharged NCNT electrodes (Figure S7). To our best knowledge, these unique morphologies of discharge products of SABs have not been reported so far. However, it is recently reported that in a LAB with RuO_2 nanoparticle-coated CNTs as air electrode, the discharge products grew uniformly on the >surface of the CNT [21], which showed an extremely similar core-shell morphology as the discharge products of NCNT air electrodes for SABs. The mechanism of the layer-by-layer growth of the discharge products on the RuO_2-CNT air electrode for LABs was believed to be promoted by the RuO_2 nanoparticles, forming a poorly crystalline Li_2O_2 layer on the CNTs [21]. It is also claimed that this uniformly formed Li_2O_2 structure provided a large contact area, which can be easily decomposed. Analogously, the sodium oxide nanorods formed on the NCNTs under high current densities have a similar structure to those of the discharge products Li_2O_2

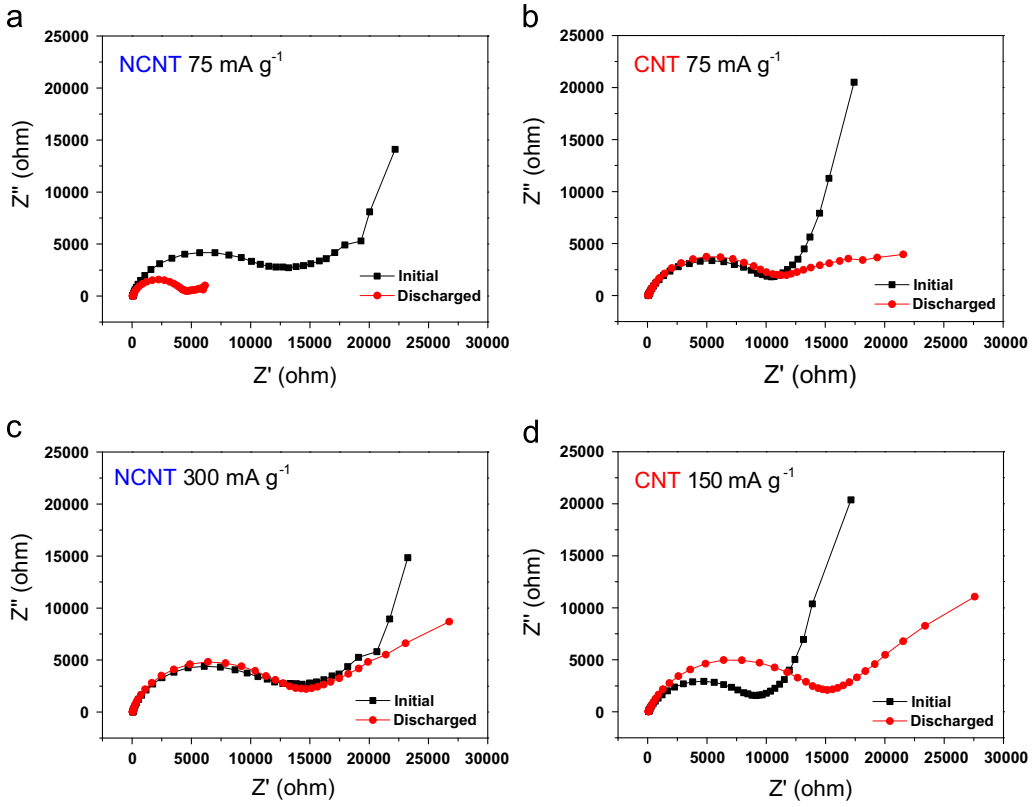

Figure 6 Electrochemical impedance spectroscopy of the Na-air batteries using NCNT (a, b) and CNT (c, d) air electrodes at low (a, c) and high (b, d) current rates. Both EIS spectra of each cell at initial and discharged states are recorded and shown, respectively.

grown on the CNT@RuO_2 core-shell air electrodes [22]. According to the first-principles calculation [36], NCNTs present a higher structural stability in the ORR process and better catalytic activity for the ORR process than both pristine and Pt-doped CNTs. It can therefore be inferred that the N-doped sites and defects in NCNTs, which have been widely believed to be the catalyst active sites for promoting ORR and OER processes, may play a similar role as the precious metal oxide RuO_2-doped CNTs, resulting in these unique structures and fascinating discharge product morphologies for SABs. Moreover, it is worthy to note that C and N elements are both naturally abundant, making NCNT air electrode highly greatly favorable for the feasibility of practical SAB applications. Moreover, compared with the irregularly shaped products on pristine CNT electrodes, the discharge products that adherently grew on the surface of NCNT electrodes can diminish the polarization and enhance the diffusion of oxygen gas during the charging and discharging processes.

In order to further clarify the role of the catalytic activities and the morphology of discharge products playing in the performance of SABs, EIS for the SABs with NCNT and CNT air electrode were recorded before and after discharging at different current rates, and the results are shown in Figure 6. The Nyquist plots of initial NCNTs and CNTs electrodes display similar shapes, which combine depressed semicircles at high frequencies attributed to the combination of charge-transfer resistance (Rct) with a constant phase element (CPE) standing for the surface double-layer capacitance, and linear spike at low frequencies, which can be described as semi-finite Warburg impedance and related to the diffusion of oxygen. It can be observed that the Rct of initial CNT air electrodes are lower than those of initial NCNT air electrodes, which might be contributed by the favored pore distribution of the CNTs comparing to NCNTs. However, the EIS of the discharged SABs with NCNT and CNT air electrode at different current densities have all shown different characteristics. Surprisingly, the charge-transfer resistance of NCNT air electrode sharply dropped by 80% after discharged under a low current density of 75 mA g^{-1} (Figure 6(a)). Considering the fact that the core-shell structure of discharge product of NCNT air electrode, it might imply that charge-transfer reaction could be greatly favored on the surface of sodium oxides. This phenomenon is also consistent with the fact that Na_2O_2 discharge products tend to exhibit a layer structure in previous report [12]. In addition, no obvious Rct change can be observed between the EIS of NCNT air electrode before and after discharged at a high current density of 300 mA g^{-1} (Figure 6(c)). In contrast, the EIS of CNT air electrode discharge at a low current density presents a close resistance compared with that of the initial CNT electrode (Figure 6(b)). However, when discharged at a relatively high current density of 150 mA g^{-1}, the resistance of the SAB with CNT air electrode increased by around 50% (Figure 6(d)). The significant increasing of Rct of CNT air electrode should be related to the accumulation of discharge products on the top of the electrode, blocking furthur oxygen and ion transportation to the surface of CNTs. These EIS data are consistent with the fact that SABs with NCNT air electrodes have shown good electrochemical performance under low and high current densities, while the capacities of SABs with CNT

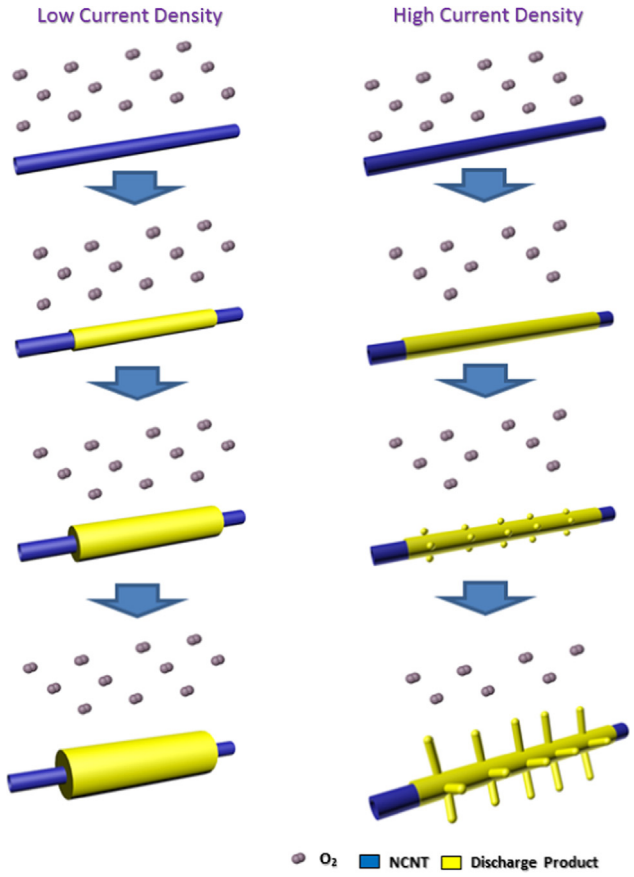

Scheme 1 Schematic diagram of the growth mechanism of discharge products on NCNT air electrodes in sodium-air batteries .

air electrode can only work under low current densities, whose capacities quickly decrease as the current densities increase.

Based on the above experimental data and analysis, the growth mechanism of the discharge products of SABs with NCNTs air electrodes are depicted in Scheme 1. Under low current densities, the NCNT air electrode is discharged under the condition close to thermodynamic equilibrium. The reaction kinetics are controlled by charge transfer. The active nitrogen-doped sites enable the fast oxygen reduction processes. In this case, the discharge products NaO_2 or Na_2O_2 gradually accumulate layer by layer near the surface of NCNTs to form the unique core–shell structure. On the other hand, under high current densities, oxygen gas transportation becomes the determining factor in the discharge process of SABs. In other words, the electrochemical reaction is controlled by diffusion. In this case, the discharge products tend to vertically grow to form the nanorods on the NCNTs following the diffusion route of oxygen, which is similar to those observed in LABs [37]. However, in the case of CNT air electrode, due to the poorer catalytic activities of CNTs, the discharge products of CNT air electrodes are not favored to selectively grow near the surface of CNTs. As a result, the discharge products tend to grow randomly. These differences between the morphologies of discharge products are also critical in the charging process. The regular grown discharge products on NCNT electrodes leave abundant internal spacing among the air electrode, enabling easy mass transportation and oxygen removal. However, the irregular discharge products on CNT electrodes clog the outer surface of air electrode and block mass transportation, which results in their poor electrochemical behavior. This evidence implies the importance of the design of air electrodes and the control of discharge product morphology for the long life cycling of SABs.

Overall, the present study demonstrates the fabrication of NCNT air electrodes and their superior electrochemical performance as air electrodes for sodium-air batteries compared to CNT air electrodes fabricated from a similar procedure. The results suggest that the design of the air electrode, as well as the morphologies of the discharge products, is critical to the cyclic stability of a sodium-air battery. NCNTs also shows improved catalytic activities toward ORR and OER processes in the cell. Uniform discharge product dispersion on the NCNT air electrodes allows for oxygen and Na-ion transportation in subsequent cycling. Meanwhile, further investigation on the understanding of sodium air batteries system with NCNT electrodes is still in progress in our research group.

Conclusion

In summary, we reported the fabrication of self-stacked NCNT air electrodes and their superior electrochemical performance at high current rates along with extended cyclic performance, in comparison to their CNT counterparts. This improvement not only is a result of the elevated catalytic activity of NCNTs due to introducing nitrogen atom doping sites, but also benefits from the uniform dispersion of discharge products formed on the surface of the NCNT network, whose structure enables rapid and unhindered oxygen and sodium ion injection and removal during cycling. Our results indicate that NCNT air electrodes can be considered as a promising candidate for sodium-air batteries. It is also implied that controlling the favorable morphology of the discharge product is of great importance in the exploration and evaluation of novel air electrode materials in the future.

Acknowledgments

This research was supported by the Natural Science and Engineering Research Council of Canada (NSERC), the Canada Research Chair Program (CRC), the Canada Foundation for Innovation (CFI), and the University of Western Ontario (UWO).

Appendix A. Supporting information

Supplementary data associated with this article can be found in the online version at http://dx.doi.org/10.1016/j.nanoen.2015.01.018.

References

[1] H.D. Yoo, E. Markevich, G. Salitra, D. Sharon, D. Aurbach, Mater. Today 17 (2014) 110–121.
[2] K. Abraham, Z. Jiang, J. Electrochem. Soc. 143 (1996) 1–5.

[3] Z.Q. Peng, S.A. Freunberger, Y.H. Chen, P.G. Bruce, Science 337 (2012) 563–566.
[4] P.G. Bruce, S.A. Freunberger, L.J. Hardwick, J.M. Tarascon, Nat. Mater. 11 (2012) 19–29.
[5] H.G. Jung, J. Hassoun, J.B. Park, Y.K. Sun, B. Scrosati, Nat. Chem. 4 (2012) 579–583.
[6] J. Wang, Y. Li, X. Sun, Nano Energy 2 (2013) 443–467.
[7] E. Peled, D. Golodnitsky, H. Mazor, M. Goor, S. Avshalomov, J. Power Sources 196 (2011) 6835–6840.
[8] Q. Sun, Y. Yang, Z. Fu, Electrochem. Commun. 16 (2012) 22–25.
[9] P. Hartmann, C.L. Bender, M. Vracar, A. Katharina Dürr, A. Garsuch, J. Janek, P. Adelhelm, Nat. Mater. 12 (2013) 228–232.
[10] X. Ren, Y. Wu, J. Am. Chem. Soc. 135 (2013) 2923–2926.
[11] Z. Jian, Y. Chen, F. Li, T. Zhang, C. Liu, H. Zhou, J. Power Sources 251 (2014) 466–469.
[12] W. Liu, Q. Sun, Y. Yang, J.Y. Xie, Z.W. Fu, Chem. Commun. 49 (2013) 1951–1953.
[13] J. Kim, H. Lim, H. Gwon, K. Kang, Phys. Chem. Chem. Phys. 15 (2013) 3623–3629.
[14] P. Hartmann, C.L. Bender, J. Sann, A.K. Dürr, M. Jansen, J. Janek, P. Adelhelm, Phys. Chem. Chem. Phys. 15 (2013) 11661–11672.
[15] Y. Li, H. Yadegari, X. Li, M. Banis, R. Li, X. Sun, Chem. Commun. 49 (2013) 11731–11733.
[16] P. Hartmann, D. Grubl, H. Sommer, J. Janek, W.G. Bessler, P. Adelhelm, J. Phys. Chem. C 118 (2014) 1461–1471.
[17] C.L. Bender, P. Hartmann, M. Vračar, P. Adelhelm, J. Janek, Adv. Energy Mater., 2014, 4: 1301863. http://dx.doi.org/10.1002/aenm.201301863.
[18] B. Lee, D.H. Seo, H.D. Lim, I. Park, K.Y. Park, J. Kim, K. Kang, Chem. Mater. 26 (2014) 1048–1055.
[19] S.K. Das, S. Laub, L.A. Archer, J. Mater. Chem. A 2 (2014) 12623–12629.
[20] H.-D. Lim, K.-Y. Park, H. Song, E.Y. Jang, H. Gwon, J. Kim, Y. H. Kim, M.D. Lima, R.O. Robles, X. Lepró, R.H. Baughman, Kisuk Kang, Adv. Mater. 25 (2013) 1348–1352.
[21] E. Yilmaz, C. Yogi, K. Yamanaka, T. Ohta, H.R. Byon, Nano Lett. 13 (2013) 4679–4684.
[22] Z. Jian, P. Liu, F. Li, P. He, X. Guo, M. Chen, H. Zhou, Angew. Chem. Int. Ed. 53 (2014) 442–446.
[23] L. Xu, J. Ma, B. Li, F. Kang, J. Power Sources 255 (2014) 187–196.
[24] B.M. Gallant, D.G. Kwabi, R.R. Mitchell, J.G. Zhou, C.V. Thompson, Y. Shao-Horn, Energy Environ. Sci. 6 (2013) 2518–2528.
[25] S.H. Oh, R. Black, E. Pomerantseva, J.-H. Lee, L.F. Nazar, Nat. Chem. 4 (2012) 1004–1010.
[26] Y. Li, J. Wang, X. Li, J. Liu, D. Geng, J. Yang, R. Li, X. Sun, Electrochem. Commun. 13 (2011) 668–672.
[27] R. Mi, H. Liu, H. Wang, K.-W. Wong, J. Mei, Y. Chen, W.-M. Lau, H. Yan, Carbon 67 (2014) 744–752.
[28] X. Lin, X. Lua, T. Huang, Z. Liu, A. Yu, J. Power Sources 242 (2013) 855–859.
[29] H. Liu, Y. Zhang, R. Li, X. Sun, S. Desilets, H. Abou-Rachid, M. Jaidann, L.-S. Lussier, Carbon 48 (2010) 1498–1507.
[30] T. Zhang, H. Zhou, Nat. Commun. 4 (2013) 1817–1823.
[31] H.-K. Lim, H.-D. Lim, K.-Y. Park, D.-H. Seo, H. Gwon, J. Hong, W.A. Goddard III, H. Kim, K. Kang, J. Am. Chem. Soc. 135 (2013) 9733–9742.
[32] B.D. McCloskey, J.M. Garcia, A.C. Luntz, J. Phys. Chem. Lett. 5 (2014) 1230–1235.
[33] N. Zhao, C. Li, X. Guo, Phys. Chem. Chem. Phys. 16 (2014) 15646–15652.
[34] S. Kang, Y.F. Mo, S.P. Ong, G. Ceder, Nano Lett. 14 (2014) 1016–1020.
[35] S.K. Das, S.M. Xu, L.A. Archer, Electrochem. Commun. 27 (2013) 59–62.
[36] C.H. San, C.W. Hong, J. Electrochem. Soc. 159 (2012) K116–K121.
[37] W.-M. Liu, T.-T. Gao, Y. Yang, Q. Sun, Z.-W. Fu, Phys. Chem. Chem. Phys. 15 (2013) 15806–15810.

Dr. Qian Sun is currently a postdoctoral fellow in Prof. Dr. Xueliang (Andy) Sun's Nanomaterials and Energy Group at the University of Western Ontario, Canada. He received his B.S. degree in Chemistry in 2006, M.S. degree in Physical Chemistry in 2009, and Ph.D. degree in Applied Chemistry in 2013 under the supervision of Prof. Dr. Zheng-Wen Fu on the study of lithium/sodium-ion batteries and sodium-air batteries at Fudan University, China. He joined Prof. Sun's group in 2013 and his current research interests focus on sodium-air, sodium-sulfur, and sodium-ion batteries.

Dr. Hossein Yadegari is currently a Ph.D. candidate at Prof. Xueliang (Andy) Sun's Nanomaterials and Energy Group at the University of Western Ontario, Canada. He received his B.Sc. (applied chemistry) from Sharif University of Technology (Tehran, Iran) in 2005 and M.Sc. and Ph.D. (analytical chemistry) from K. N. Toosi university of Technology (Tehran, Iran) in 2012. His main research interests are electrochemistry of nanomaterials, electrochemical energy saving devices and electrocatalysis. His current research is focused on development of nanostructured air electrode for alkali metal-oxygen cells.

Dr. Mohammad Norouzi Banis is currently a post-doctoral fellow at Prof. Xueliang (Andy) Sun's Nanomaterials and Energy Group at the University of Western Ontario, Canada. He received his Ph.D. degree for research on synthesis and advanced characterization of nanomaterials for fuel cell application in 2012. His research interests included energy conversion, advanced nanomaterial synthesis and characterization methods such as atomic layer deposition and synchrotron based techniques.

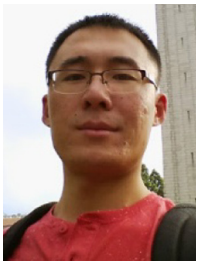

Dr. Jian Liu is a postdoctoral fellow in Dr. Jinghua Guo's group at Advanced Light Source in Lawrence Berkeley National Laboratory (LBNL, USA). He received Master degree in Materials Science and Engineering at University of Science and Technology Beijing (China) in 2009. Then he joined in Dr. Xueliang (Andy) Sun's Nanomaterials and Energy Group at University of Western Ontario (Canada) with research focus on development of advanced nanomaterials for lithium-ion battery applications, and earned his Ph.D. degree in Materials Science in August 2013. Dr. Liu has received several prestigious awards, including Mitacs Elevate Strategic Fellowship Award and NSERC Postdoctoral Fellowship. His research interests are associated with design, synthesis, and characterization of advanced nanomaterials for clean energy storage and conversion. Currently, his focus is on development of novel electrode materials by atomic layer deposition and in-situ/in-operando soft X-ray spectroscopy study of lithium-ion and sodium-ion batteries.

Biwei Xiao is a Ph.D. candidate in Prof. Xueliang (Andy) Sun's group at the University of Western Ontario, Canada. He received his B. Eng degree from Sichuan University, China, in 2011. He started his master study in Prof. Sun's group in Jan. 2012 and transferred to a Ph.D. candidate in 2013. His research area mainly includes carbon nanotubes, synthesis and surface modification of cathode materials for lithium ion batteries and synchrotron radiation technique characterization and analysis of battery materials.

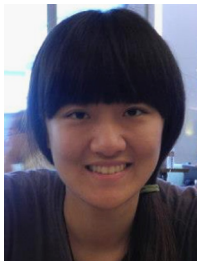

Biqiong Wang is currently a Ph.D. candidate in Prof. Xueliang (Andy) Sun's Nanomaterials and Energy Group at the University of Western Ontario, Canada. She received her Bachelor degree in Materials Science in 2012 at the City University of Hong Kong. Her research interests are associated with the application of atomic layer deposition in all-solid-state batteries. She is also co-supervised by Prof. T. K. Sham from Chemistry Department in the University of Western Ontario. Part of her work is related to the study of energy materials via synchrontron radiation.

Stephen Lawes is currently a Master's student in Professor Xueliang (Andy) Sun's Nanomaterials and Energy Group at the University of Western Ontario, Canada. He received his Bachelor of Applied Science in Nanotechnology Engineering from the University of Waterloo, Canada, in 2013. His current research focuses on developing printable batteries using inkjet and 3D printing techniques.

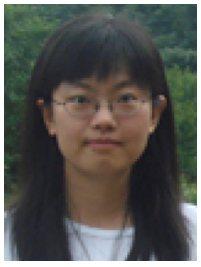

Xia Li is currently a Ph.D. candidate in Prof. Xueliang (Andy) Sun's Nanomaterials and Energy Group at the University of Western Ontario, Canada. She received her Bachelor degree at Dalian University of Technology, China, and Master degree at Nankai University, China. Her current research interests focus on development of advanced nanomaterials for lithium-sulfur batteries.

Ruying Li is a research engineer at Prof. Xueliang (Andy) Sun's Nanomaterial and Energy Group at the University of Western Ontario, Canada. She received her master degree in Material Chemistry under the direction of Prof. George Thompson in 1999 at University of Manchester, UK, followed by work as a research assistant under the direction of Prof. Keith Mitchell at the University of British Columbia and under the direction of Prof. Jean-Pol Dodelet at l'Institut national de la recherché scientifique (INRS), Canada. Her current research interests are associated with synthesis and characterization of nanomaterials for electrochemical energy storage and conversion.

Professor Xueliang (Andy) Sun is a Senior Canada Research Chair (Tier 1) and a Full Professor at the University of Western Ontario, Canada. Dr. Sun received his Ph.D. in Materials Chemistry under the direction of Prof. George Thompson in 1999 at the University of Manchester, UK, followed by work as a postdoctoral fellow under the direction of Prof. Keith Mitchell at the University of British Columbia, Canada and as a Research Associate under the direction of Prof. Jean-Pol Dodelet at l'Institut national de la recherche scientifique (INRS), Canada. His current research interests are associated with synthesis of advanced nanomaterials for electrochemical energy storage and conversion including PEM fuel cells, lithium ion batteries and metal-air batteries.